Low-parameter linear model to activate the flexibility of the building thermal mass in energy system optimization

Magnus Askeland [a,*], Laurent Georges [b], Magnus Korpås [c]

[a] *Energy Systems, SINTEF Energy Research, Trondheim, Norway*
[b] *Department of Energy and Process Engineering, Norwegian University of Science and Technology, Trondheim, Norway*
[c] *Department of Electric Power Engineering, Norwegian University of Science and Technology, Trondheim, Norway*

ARTICLE INFO

ABSTRACT

As buildings are becoming an integrated part of the energy system, the potential activation of the thermal mass as a source of flexibility needs to be considered in energy system modeling. Since energy system models represent larger and integrated systems, often as linear programs, the thermal mass activation of buildings needs to be formulated accordingly to be included as a flexibility asset in the energy system optimization problem. The article provides a linear model of the energy stored in the building thermal mass compared to a reference operation scenario without demand response. This formulation in relative terms significantly reduces the number of model parameters to be identified using field measurements and enables the analysis of the aggregated energy flexibility in energy system models. The thermal mass activation is demonstrated in a case study which also includes validation. In addition, a comparison of the thermal mass activation and batteries is made. It is concluded that the provided linear deviation-based formulation is appropriate for representing the potential of flexibility provision from the thermal mass in buildings for the purpose of energy system planning.

1. Introduction

1.1. Background

As the energy supply shifts towards renewable generation resources, the need for flexibility throughout the system increases [1]. For the building level, one potential source of flexibility is the thermal mass. According to IEA EBC Annex 67, the energy flexibility of a building is the ability to manage its demand and generation according to local climate conditions, user needs, and energy network requirements [2].

Energy system models are used to plan the optimal operation and investment strategies for energy systems of different temporal and spatial scales. Energy system models can either focus on a single energy carrier such as electricity, or multiple energy carriers possible involving also district heating and more. One example is the energy hub modeling concept initially proposed by Geidl and Andersson [3]. The energy hub approach is used in several scientific studies that focus on optimizing community-scale energy systems, e.g., [4–7]. The papers [8,9] provide an overview of scientific contributions based on the energy hub approach. Since demand is usually represented by fixed load profiles, energy system models largely rely on flexibility in the layers before the

final use of energy and variations in load patterns have traditionally been handled by generation or storage technologies. For example, the authors in [10] utilize a varying temperature in the district heating grid as an energy storage, but do not include the thermal mass of the buildings as a potential source of flexibility, while the authors in [11] claim that the thermal inertia of buildings is 1000 times higher than that of the water in district heating networks.

By utilizing the potential of thermal mass within comfort limits, it has been shown that the heat load profiles can be adapted to provide significant demand response, see, e.g., [12–18]. As buildings become an integrated part of smart energy systems [19], it is increasingly important to have a good representation of buildings' thermal flexibility in energy system optimization models. Energy system models must consider buildings as a part of a complex system, and therefore the modeling detail must be kept at a reasonable level while maintaining enough accuracy. One main obstacle is that the mathematical structure of detailed building models typically includes nonlinear relationships and other properties that is not applicable within the structure of energy system models. Therefore, since linear mathematical formulations are used in the majority of energy system models, there is a need for a compatible formulation of building thermal mass flexibility.

1.2. Research context

The idea of representing flexibility in the thermal mass of buildings in energy planning tools have been pursued by several authors in the recent years [20–25]. This article extends our preliminary paper [26], where we made a distinction between two main categories of thermal mass flexibility models:

- Methods that evaluate the absolute value of the indoor temperature (category A).
- Methods that evaluate the change of indoor temperature compared to a reference scenario (category B).

Within category A, thermal comfort criteria are typically expressed as a range of indoor temperature bounded by a minimum and maximum threshold. Modeling of the indoor temperature in absolute value requires a model that incorporate many complex physical phenomena such as solar irradiation and heating and ventilation system dynamics. Regarding the energy system perspective, several studies includes linear modeling of the building thermal mass. [27–30] used a linear first-order grey-box model, Salpakari et al. [31] used a linear second-order grey-box model and Nguyen et al. [32] used a linear third-order grey-box model. All these models considered the building as a single thermal zone (i.e., monozone) while Baader et al. [33] used a linear grey-box model of a room assuming adiabatic internal walls. Pattheuw et al. [34,35] considered a linear five-order two-zone grey-box model. Given the complex representation of an individual building, a recent contribution of Hedegaard et al. [36] proposes a clustering method to reduce the number of buildings in the optimization and thus the computational time.

Reformulating the problem in relative terms (category B) leads to important simplifications. The change of indoor temperature compared to the reference scenario is described as a function of the shift in space-heating power compared to the reference scenario. Hence, the indoor temperature deviation represents the state of charge. Based on the idea that the building dynamics is complicated but the thermal mass energy storage only corresponds to a limited indoor temperature change, the building dynamics are linearized around the reference scenario where a linear model should be accurate enough for operational deviations. A main advantage of the method is that it only models the relation between the change of space-heating power and the change of indoor temperature, without the complex modeling of the internal and solar gains. This idea has been proposed by Kensby et al. [12] and Romanchenko et al. [21] in the context of building thermal mass in district heating.

For the system planning aspect it is crucial to represent the load profiles along with a linear representation of the flexibility. The authors in [13] characterize the storage potential of several building types in relative terms, but specify the identified parameters independent of each other such the characterization is not suited for use in optimization models. A simplified flexibility function is proposed by the authors in [23], which propose a method for characterizing the load response to a penalty signal which can be used for determining how boundary conditions affect the load profile, but does not formulate the effect of load deviations on the internal state of the building.

In contrast to these related papers, our relation between load deviation and temperature deviation enables linear optimization of second-order thermal dynamics of buildings to be directly included in the optimization of larger energy systems.

1.3. Research contributions

There is a need to bridge the gap between building-specific and energy system models to evaluate the value of building flexibility in the energy system and determine how building flexibility can affect energy system design and operation. Compared to the existing literature discussed in section 1.2, the novelty of this paper lies in the formulation for the available energy storage in the thermal mass of buildings based on the deviation of the space heating relative to a reference operational pattern. We demonstrate how this approach can be utilized in energy system optimization by conducting a case study where the building flexibility is used to optimize the energy flow at the local system level. This article builds on [26], where a linearized building flexibility formulation was suggested. The main contributions of this article are:

- Providing a linear formulation for space heating flexibility with a limited number of model parameters to facilitate their calibration and the aggregation of several buildings with the same parameter values. At the same time, this model can be directly implemented in linear optimization problems.
- Represent the thermal mass of buildings as an energy storage in an energy system optimization problem.
- Conduct an illustrative case study to evaluate the effect of thermal mass activation in a local energy system under different operational conditions. Using this test case, compare the storage capacity of the building thermal mass and batteries.

1.4. Paper structure

Following this introduction, this paper is structured as follows. First, the methodology for representing the thermal response of buildings is described in section 2, which also includes the formulation of an energy system model incorporating the activation of building thermal mass. Section 3 presents a case study focusing on thermal mass activation of two archetypes in the context of an illustrative energy system model. Thereafter, results and discussions provided in section 4 before conclusions are drawn in section 5.

2. Method

2.1. Linearization of building dynamics

The modeling of building dynamics includes the building envelope and the heat emitter, excluding its local control (e.g., a thermostatic valve). The objective is to obtain a linear model to represent the relation between the increase of power delivered to the heat emitter and the increase of indoor temperature.

With these boundaries, the building dynamics can be described by a nonlinear state-space model:

$$\dot{\boldsymbol{X}}(t) = F_x(\boldsymbol{X}(t), \boldsymbol{U}(t)) \tag{1}$$

$$T^i(t) = Y(t) = F_y(\boldsymbol{X}(t)) \tag{2}$$

where $\boldsymbol{X}$ is the state vector, Y is the scalar output, namely the indoor temperature, T^i, and $\boldsymbol{U}$ is the input vector with the outdoor temperature (T^{out}), the wind speed, two components of the solar irradiation, such as the global irradiation on a horizontal plane ($I_{g,h}$) and the beam irradiation on a normal plane ($I_{b,n}$), the power of the internal gains (P^{int}) and the power emitted by the heat emission subsystem (P^e). The flexible operation can be expressed as a deviation from a reference scenario. As P^e is the only input that deviates from the reference scenario, $\Delta \boldsymbol{U}(t)$ simplifies into $\Delta P^e(t)$:

$$\boldsymbol{X}(t) = \boldsymbol{X}^{ref}(t) + \Delta \boldsymbol{X}(t) \tag{3}$$

$$T^i(t) = T^{i,ref}(t) + \Delta T^i(t) \tag{4}$$

$$\boldsymbol{U}(t) = \boldsymbol{U}^{ref}(t) + \Delta P^e(t) \tag{5}$$

The nonlinear state-space model can then be linearized around this reference scenario:

$$\Delta \dot{\boldsymbol{X}}(t) = \left. \frac{\partial F_x}{\partial \boldsymbol{X}} \right|_{ref} \Delta \boldsymbol{X}(t) + \left. \frac{\partial F_x}{\partial P^e} \right|_{ref} \Delta P^e(t) = A \Delta \boldsymbol{X}(t) + B \Delta P^e(t) \tag{6}$$

$$\Delta T^i(t) = \frac{\partial F_y}{\partial \boldsymbol{X}}\bigg|_{ref} \Delta \boldsymbol{X}(t) = C \Delta \boldsymbol{X}(t) \tag{7}$$

This is a linear state-space model with a single input and a single output (SISO), ΔP^e and ΔT^i, respectively. It has the corresponding transfer function $H(s)$:

$$H(s) = C(sI - A)^{-1}B \tag{8}$$

Based on this, these important characteristics can be expressed:

- Compared to the original nonlinear system of equations in eq. (1) and eq. (2), the linearized model only models the influence of ΔP^e on ΔT^i and phenomena that are complex to model, like solar gains and internal gains, are excluded, meaning that these phenomena are already taken into account in the reference scenario.
- Even though the deviations are evaluated with a linear model, the reference scenario can still originate from a nonlinear model.
- The formulation is better adapted for residential buildings where the space-heating is performed with a heat emitter located in the room. When the space-heating is a combination of ventilation heating and local heat emitters, the thermal dynamics can be fundamentally non-linear, especially for variable air volume (VAV) ventilation systems, typical of non-residential buildings, like offices. However, in some practical applications, the system behavior remains close to linear over a large range of operating conditions (e.g., for constant air volume systems, CAV). Therefore, the linear model formulation is expected to remain valid.

2.2. Modeling of the transfer function

An abundant literature has demonstrated that a first-order model is not sufficient to capture the thermal dynamics of the building envelope, see, e.g., [12,21,37]. A second-order model with fast and slow dynamics have demonstrated to give good simulation performance.

As a complement to the methodology, we propose to characterize energy flexibility using a step response. It means that ΔP^e in eq. (6) is taken as a step function. The step response $\Delta T^i(t)$ in eq. (9) will represent the signature of the building energy flexibility potential. Several authors have stressed the close relationship between the thermal mass energy flexibility and its time constants [12,21,23,38]. In the same way, the step response is parameterized as a function of the time constants, meaning two constants for a second-order model:

$$\Delta T^i(t) = [\alpha(1 - \exp(-t/\tau_1)) + (1 - \alpha)(1 - \exp(-t/\tau_2))]\Delta T^i(\infty) \tag{9}$$

$$\Delta T^i(\infty) = \Delta P^e / U_{tot} \tag{10}$$

U_{tot} is the overall heat transfer coefficient and a steady-state performance indicator, τ_1 and τ_2 are the two building time constants, and α is a weighting factor for the relative importance of each time constant in the step response. This parameterization of the step response is expected to be more universal and not vary much within a given building category or archetype.

The step response can be converted into a linear state-space model using different methods. For simplicity, the conversion will be done directly using the transfer function $H(s)$. The time constants are directly related to the eigenvalues of the linear system:

$$\lambda_1 = -1/\tau_1 < 0, \quad \lambda_2 = -1/\tau_2 < 0, \quad \lambda_1 > \lambda_2 \tag{11}$$

To simplify the notation, a weighted eigenvalue can be defined:

$$\lambda_m = \alpha \lambda_1 + (1 - \alpha)\lambda_2 \tag{12}$$

The transfer function (eq. (8)) corresponding to the step function (eq. (9)) then has the following expression:

$$H(s) = \frac{-\lambda_m s + \lambda_1 \lambda_2}{(s^2 - (\lambda_1 + \lambda_2)s + \lambda_1 \lambda_2)U_{tot}} \tag{13}$$

The transfer function can be converted back into the physical domain, firstly into a second-order ordinary differential equation and, afterwards, into a second-order linear state-space model:

$$A = \begin{bmatrix} 0 & 1 \\ -(\lambda_1 \lambda_2) & (\lambda_1 + \lambda_2) \end{bmatrix} \tag{14}$$

$$B = \begin{bmatrix} -\lambda_m/U_{tot} \\ (\lambda_1 \lambda_2 - \lambda_m(\lambda_1 + \lambda_2))/U_{tot} \end{bmatrix} \tag{15}$$

$$C = \begin{bmatrix} 1 \\ 0 \end{bmatrix} \tag{16}$$

2.3. Aggregation of several buildings

In an energy planning tool, a node typically represents the load of several buildings. Using the proposed approach, all buildings having the same parameters (U_{tot}, τ_1, τ_2 and α) can be aggregated together in a single node even though the occupant behavior and the weather conditions are different for each building. If N similar buildings are aggregated together in a single node, an equal increase of indoor temperature ΔT^i will take place in each of the N buildings if the same increase of power ΔP^e is applied. In the energy planning tool, an optimization constraint is set on ΔT^i and the change of power at aggregated level, $\Delta P^{e,tot}$, is divided equally between the N buildings of the node:

$$\Delta P^e = \Delta P^{e,tot}/N \tag{17}$$

2.4. Parameter identification

Different methods can be used to calibrate the parameters of the model for a specific residential building. Parameters can be identified using virtual experiments in building performance simulation (BPS). In our previous publication [26], two alternative identification approaches based on BPS are introduced and compared. However, the methodology would be easier to deploy if the model parameters could be calibrated using field measurements. At first sight, it is a challenging task as it is complex to measure a deviation of indoor temperature and space-power compared to a reference scenario, as both scenarios should be measured for the same boundary conditions. However, two approaches enable to circumvent the problem.

In the first approach a standard second-order grey-box model can be identified, see, e.g., [39,40]. The grey-box model expresses the conservation of energy and is often formulated as a resistance-capacitance (RC) network. It relates the indoor temperature in absolute terms (T^i) to all the input parameters (**U**). This is linear version of eq. (1) and eq. (2); a linear state-space model. The parameters (U_{tot}, τ_1, τ_2 and α) can be extracted from the transfer function of the grey-box model between T^i and P^e. However, this approach needs a considerable amount of measurement data. To limit these field measurements, the method can be applied to a limited number of building archetypes. For the second approach, several methods have been developed to evaluate the overall heat transfer coefficient (U_{tot}) of a building using in-situ measurements, such as the co-heating test or the PStar method [41]. However, these methods require several days or even weeks of measurements. To solve this time constraint, the QUB method [42] has been recently proposed to give a reasonable accurate estimation of U_{tot} with short-term measurements, up to less than one night. The experiments are performed during nighttime to avoid the influence of solar gains and the building is ideally unoccupied to avoid internal gains. In addition, the experiment requires measuring the space-heating power P^e. The prediction accuracy using the QUB method reported in [42] is in the range of +/- 20%. Regarding the building time constants (τ_1, τ_2), the recent paper of Palmer Real et al. [38] proposes to identify them during the space-heating temperature setback during nighttime, when internal and solar gains should be negligible and the space-heating power equal to zero. They develop a stochastic approach to identify the time constants based on the indoor temperature decay curve. The indoor temperature decay
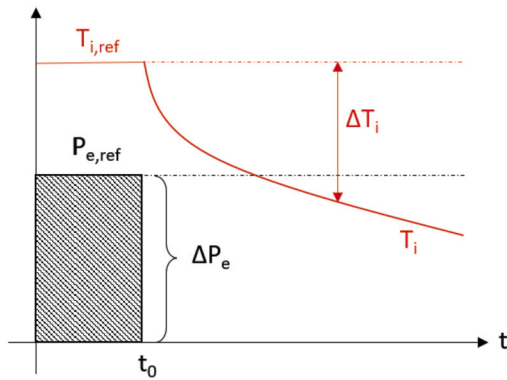
Fig. 1. Identification procedure using night temperature setback.

Fig. 2. Topology of the considered system.

is recorded every 10 during several nights to identify the two time constants. However, the approach is based on a monozone model and it assumes that the two states of the model, roughly representing the indoor air and the wall temperatures, are equal at the beginning of the temperature decay.

In conclusion, recent developments in the characterization of the building performance using in-situ measurements enables to give a fair estimate of the (U_{tot}, τ_1, τ_2) based on limited measurements. In our work, we assume that the overall heat transfer coefficient U_{tot} is available using one these methods, like QUB. However, for the other parameters, an alternative method is introduced. In the method proposed by Palmer Real et al. [38], the building is monozone while the temperature in residential buildings can often not be assumed equal in all the rooms. For instance, in Norway, occupants prefer cold temperatures in bedrooms [43]. Therefore, we rather use a method that can both consider buildings as monozone but also different room temperatures. The principle is shown in Fig. 1.

It is assumed that the building is in a quasi-steady state when the night temperature setback starts at time t_0 [44]. The entire identification procedure happens during nighttime to avoid solar gains. It is also assumed that users are not active before the temperature setback as they will move to bedrooms so that internal gains are negligible. As in Palmer Real et al. [38], it is assumed that the outdoor temperature does not vary significantly during the temperature decay period so that it can be assumed constant. The indoor temperature and space-heating power before the night temperature setback is then taken as the reference scenario. When the setback starts, the space-heating power goes to zero so that ΔP^e is equal to $P_{e,ref}$. The parameters (τ_1, τ_2 and α) are identified by curve-fitting of the indoor temperature decay ΔT^i measured during several nights using eq. (9) and eq. (10). When the method is applied for the entire building, T^i is the volume-averaged air temperature of all the rooms and P^e is the total space-heating power. U_{tot} is then the overall heat transfer coefficient of the building with all the rooms at an equal temperature. When applied at the room level, T^i is the room-averaged air temperature and P^e is the space-heating power of the local heat emitter. U_{tot} is then the overall heat transfer coefficient of the room with the neighboring rooms unheated.

The new procedure is based on many assumptions. However, the method is expected to be reasonably accurate to be used to evaluate the energy flexibility of the building thermal mass in an energy planning tool. The accuracy is tested against detailed thermal dynamic simulations in building performance simulation package using a test case introduced in section 3.

2.5. Energy system model

To investigate the potential of space heating flexibility in a broader context, an energy system model as described by Fig. 2 is formulated as a linear optimization problem in Julia [45]. The optimization problem for the energy system model is solved using the CPLEX solver on a server
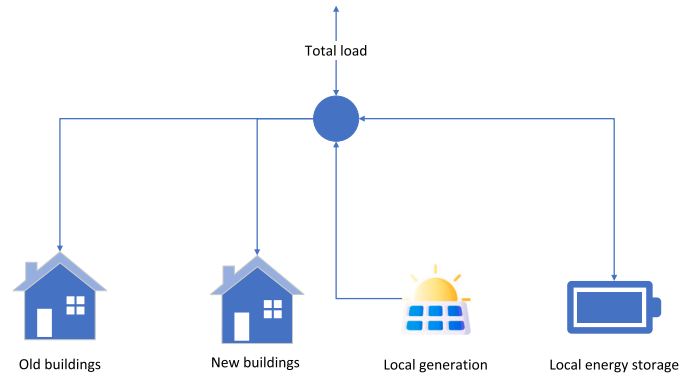
with Intel Xeon 6240 quad core CPU and 64 GB of RAM. A total of 42 different cases are computed to produce the analysis in this paper, and the solution time for each computation is varying between 1-2 minutes.

The system consists of buildings of different insulation levels, local generation resources, and energy storage. For simplicity, it is assumed that all energy is supplied through electricity and that the local system interacts with the external grid as one entity.

2.5.1. Objective function

The optimization goal is to minimize the total cost of energy procurement according to eq. (18). The costs are based on the amount of energy, and the grid capacity usage. The cost of importing energy consists of the electricity market price (MP_t) in addition to the distribution grid import tariff (VI). Energy exports are remunerated based on the market price subtracted the export tariff (VE).[1] Finally, a capacity-based network tariff is imposed (CT). To allow the model to have a temporal resolution different from one hour, the parameter ΔI represents the duration of each time step.

$$Min : \sum_{t=1}^{I}(imp_t * \Delta I * (MP_t + VI) - exp_t * \Delta I * (MP_t - VE)) + cap * CT$$

(18)

2.5.2. Energy balance

The energy balance for the local system is described by eq. (19). The net imports of energy equals the total building load, energy storage operation and generation from local energy resources. The building load for each category (ϕ) is split into a fixed part representing nonflexible loads such as noncontrollable heating, lights and other equipment and a flexible part representing the controllable space heating.

$$imp_t - exp_t = \sum_{\phi=1}^{\Phi}(P_{\phi,t}^{fix} + P_{\phi,t}^{e}) + ch_t - dis_t - gen_t \quad \forall t$$

(19)

2.5.3. Grid capacity measurement

The capacity usage is based on settlement periods (β) with a duration (ΔB) that can be larger than the temporal resolution of the overall optimization problem (ΔI). The capacity used during each settlement period is computed as an average of the grid capacity usage during the period and the billable capacity usage is based on the settlement period with the highest usage according to eq. (20).

$$cap \geq \sum_{t=\beta}^{t<\beta+1}(imp_t + exp_t) * \frac{\Delta I}{\Delta B} \quad \forall \beta$$

(20)

---

[1] The export tariff can be zero or negative.

<div style="border:1px solid black; padding:10px;">

Nomenclature for energy system model

Sets

$\beta \in B$	Capacity settlement periods	
$\iota \in I$	Time steps	
$\phi \in \Phi$	Building categories	

Parameters

ΔI	Time step duration	[h]
C^E	Generation capacity	[kWp]
C^S	Energy storage size	[kWh]
C^{ch}	Energy storage charging capacity	[kW/kWh]
C^{dis}	Energy storage discharging capacity	[kW/kWh]
CT	Distribution grid capacity tariff	[EUR/kWh/h]
G_ι	Energy generation potential	[kW/kWp]
L	Energy storage converter losses	[%]
MP_ι	Electricity market price	[EUR/kWh]
$P^{fix}_{\phi,\iota}$	Nonflexible load	[kW]
$P^{e,ref}_{\phi,\iota}$	Reference flexible heat load	[kW]
P^{max}_ϕ	Flexible heat source capacity	[kW]

R	Energy storage self-discharge rate	[%/h]
$T^{max}_{\phi,\iota}$	Maximum temperature	[°C]
$T^{min}_{\phi,\iota}$	Minimum temperature	[°C]
$T^{ref}_{\phi,\iota}$	Reference temperature	[°C]
VE	Distribution grid export tariff	[EUR/kWh]
VI	Distribution grid import tariff	[EUR/kWh]

Variables

$\Delta P^e_{\phi,\iota}$	Thermal mass activation	[kW]
$\Delta T_{\phi,\iota}$	Temperature deviation	[°C]
cap	Grid capacity usage	[kWh/h]
ch_ι	Battery charging	[kW]
dis_ι	Battery discharging	[kW]
exp_ι	Energy exports	[kWh/h]
gen_ι	Generation from local energy resources	[kW]
imp_ι	Energy imports	[kWh/h]
$P^e_{\phi,\iota}$	Flexible space heating load	[kW]
s_ι	Energy storage charge level	[kWh]

</div>

2.5.4. Battery

The battery stores energy for use in later periods. The charge level in the next period ($s_{\iota+1}$) is equal to the charge level during the current period (s_ι) and the amount of energy charged to or discharged from the battery according to eq. (21). Losses are included through a self-discharge parameter (R) and converter losses when charging or discharging the battery (L). To handle the boundary condition in the last time step, a round-coupling to the first time step is included according to eq. (22).

$$s_{\iota+1} = s_\iota * (1 - R * \Delta I) + ch_\iota * \Delta I * (1 - L) - dis_\iota * \Delta I * (1 + L) \quad \forall \iota < I \tag{21}$$

$$s_1 = s_\iota * (1 - R * \Delta I) + ch_\iota * \Delta I * (1 - L) - dis_\iota * \Delta I * (1 + L) \quad \forall \iota = I \tag{22}$$

The amount of energy that can be stored is limited to the battery size (C^S) according to eq. (23), while the charging and discharging capacity is given as a fraction of the storage capacity in eqs. (24) and (25).

$$s_\iota \leq C^S \quad \forall \iota \tag{23}$$

$$ch_\iota \leq C^{ch} * C^S \quad \forall \iota \tag{24}$$

$$dis_\iota \leq C^{dis} * C^S \quad \forall \iota \tag{25}$$

2.5.5. Energy generation

Local energy generation from for example a PV system is formulated according to eq. (26). Generation during each time step is based on a generation profile (G_ι) that describes the potential generation for each unit of capacity (C^E).

$$gen_\iota \leq G_\iota * C^E \quad \forall \iota \tag{26}$$

2.6. Linearized building flexibility model as an energy storage

We represent the space heating as the reference flexible heat load $P^{e,ref}_{\phi,\iota}$ adjusted by the thermal mass activation variable $\Delta P^e_{\phi,\iota}$:

$$P^e_{\phi,\iota} = P^{e,ref}_{\phi,\iota} + \Delta P^e_{\phi,\iota} \quad \forall \phi,\iota \tag{27}$$

Since the energy system model is implemented with discrete time steps, the matrices eq. (14), eq. (15), and eq. (16) are discretized through the ControlSystems package [46] with a time step duration of 0.02 hours. This yields the following relation between temperature deviation ($\Delta T_{\phi,\iota}$) and thermal mass activation:

$$\Delta T^{(1)}_{\phi,\iota+1} = \Delta T^{(1)}_\phi * A^{(1,1)}_\phi + \Delta T^{(2)}_\phi * A^{(1,2)}_\phi + \Delta P^e_{\phi,\iota} * B^{(1)}_\phi \quad \forall \phi, \iota < I \tag{28}$$

$$\Delta T^{(2)}_{\phi,\iota+1} = \Delta T^{(1)}_\phi * A^{(2,1)}_\phi + \Delta T^{(2)}_\phi * A^{(2,2)}_\phi + \Delta P^e_{\phi,\iota} * B^{(2)}_\phi \quad \forall \phi, \iota < I \tag{29}$$

Rather than specifying initial and final states, the building state is round-coupled from the last to the first time step. This is similar to the round-coupling of the battery:

$$\Delta T^{(1)}_{\phi,1} = \Delta T^{(1)}_{\phi,\iota} * A^{(1,1)}_\phi + \Delta T^{(2)}_{\phi,\iota} * A^{(1,2)}_\phi + \Delta P^e_{\phi,\iota} * B^{(1)}_\phi \quad \forall \phi, \iota = I \tag{30}$$

$$\Delta T^{(2)}_{\phi,1} = \Delta T^{(1)}_{\phi,\iota} * A^{(2,1)}_\Phi + \Delta T^{(2)}_{\phi,\iota} * A^{(2,2)}_\phi + \Delta P^e_{\phi,\iota} * B^{(2)}_\phi \quad \forall \phi, \iota = I \tag{31}$$

We include limits on the indoor temperature ($T^{1,ref}_{\phi,\iota} + \Delta T^1_{\phi,\iota}$). The limits need to account for situations where the reference temperature is outside the allowed interval, e.g., due to overheating issues that can arise for well insulated buildings even when the heat source is turned off. Hence, the upper limit is determined as an evaluation of the maximum of the reference temperature and the upper temperature limit while the lower limit is determined as the minimum of the reference temperature and the lower temperature limit:

$$T^{1,ref}_{\phi,\iota} + \Delta T^1_{\phi,\iota} \leq \max\{T^{ref}_{\phi,\iota}, T^{max}_{\phi,\iota}\} \quad \forall \phi,\iota \tag{32}$$

$$\min\{T^{ref}_{\phi,\iota}, T^{min}_{\phi,\iota}\} \leq T^{ref}_{\phi,\iota} + \Delta T^1_{\phi,\iota} \quad \forall \phi,\iota \tag{33}$$

There is also a limit on the maximum power from the heating source, based on it's capacity (P^{max}_ϕ):

$$P^e_{\phi,\iota} \leq P^{max}_\phi \quad \forall \phi,\iota \tag{34}$$

3. Case study setup and input data

3.1. Description of the buildings

The case of a single-family detached house as depicted in Fig. 3 is analyzed using detailed dynamic simulation in IDA ICE [47]. The building has been initially defined and implemented by Rønneseth et al. [48] and is available for different insulation levels. Some adjustments of the model have been applied by Elin Storlien [49]. The building has a heated area of 162 m^2, 81 m^2 of floor and flat roof, 222 m^2 of external walls including 32 m^2 of windows. The building is heated by electric radiators. In reality, P_e can be measured using an accurate watt meter plug. Electric radiators are here modeled as ideal heaters controlled by a PI controller. A real electric radiator has most likely an on-off control. The ratio between convection and total heat emitted is fixed to 0.6. The building is divided into three thermal zones: the ground floor with the living room, the bedrooms, and the bathroom on the first floor. Each

Fig. 3. View of the virtual 3D geometry of the building.

zone has one heat emitter. The nominal power ($P_{e,n}$) of each emitter has been sized using a design heating load simulation. The internal doors between zones have been assumed closed.

The building is constructed in wood, meaning a lightweight structure. Two different performances of the building envelope are considered. Firstly, a super-insulated version where the building complies with the Norwegian definition of the passive house (PH) standard [50]. The building then has balanced mechanical ventilation equipped with heat recovery with constant effectiveness at 85%. Second, a poorly insulated version corresponding to the Norwegian building regulation requirements of 1987, TEK87 [51]. In this case, the building has natural ventilation, here modeled as balanced mechanical ventilation without heat recovery.

Some comments should be given regarding the modeling of the building physics in IDA ICE. The tool automatically integrates a ventilation network model [52]. Pressure coefficients (C_p) have been defined on each external wall. Consequently, wind- and buoyancy-driven air infiltrations are computed. The heat conduction in walls assumes constant thermal properties for each layer of the wall, which makes it linear. However, surface convection coefficients and thermal radiation between surfaces are nonlinear. As the TEK87 is less insulated, the influence of the surface heat transfer is more important and the infiltrations are larger. Consequently, the thermal dynamics of the TEK87 building is expected to be more nonlinear than the PH. The building has no active solar shading but is surrounded by obstacles representing neighboring buildings. The influence of these obstacles on the direct solar irradiation is evaluated in detail at every time step by IDA ICE. In all simulations, the data import and export in IDA ICE are performed using a sampling time (Δt) of 6 minutes.

In the reference scenario, the set-point temperature for the living room during daytime is 21 °C for the TEK87 building and 22 °C for PH building. The night temperature setback starts at 11PM. Then, the set-point temperature is reduced to 16 °C until 7AM. A constant set-point temperature of 16 °C is applied to bedrooms. Internal gains are taken from the technical standard SN:TS3031 [53] assuming constant occupancy and the historical weather data of 2019 in Oslo has been used.

3.2. Prices and system characteristics

We consider the year 2019 both regarding prices and climatic data. Prices for the interaction with the electricity grid are provided in Table 1. The grid tariffs are based on historical prices for jointly metered systems gathered from Elvia [54], historical day-ahead electricity prices are gathered from NordPool for the Oslo area [55], and the excise tax is gathered from the Norwegian Tax Administration [56]. Notice that we present the average electricity price here, while the hourly price is used in the optimization. All prices include value-added tax of 25%.

The energy system also has some energy resources, a PV system and the possibility for a battery. Assumed technical parameters for these assets are presented in Table 2.

Table 1
Electricity costs based on historical data for 2019.

Cost component	Dec-Feb	Mar, Nov	Apr-Oct
Grid tariff (capacity) [€/kW]	18.75	10.00	2.88
Grid tariff (energy import) [€/kWh]	0.00875	0.00875	0.00488
Grid tariff (energy export) [€/kWh]	0	0	0
Electricity tax [€/kWh]	0.01979	0.01979	0.01979
Electricity price (average) [€/kWh]	0.05865	0.04341	0.05053

Table 2
Technical parameters for the system.

Parameter	Value
Converter loss (battery) [%]	5
Self-discharge (battery) [%/h]	0.1
Battery capacity [kW/kWh]	0.5
Battery capacity [kWh]	Case-dependent
PV system losses [%]	10
PV capacity [kW]	100
PV annual capacity factor [%]	9.08
PV annual generation [kWh]	79 579
Minimum temperature [°C]	$T_{\phi,t}^{1,ref}$
Maximum temperature [°C]	24
TEK87 heat power [kW]	4.44
PH heat power [kW]	1.57

PV generation for the Oslo area for 2019, assuming 10% PV system losses and directly upwards facing panels is generated by using an online tool,[2] which is based on the method presented in [57].

3.3. Operational scenarios and building scaling

Each building category has three different load types:

1. Load used for appliances.
2. Load used for non-flexible heating and domestic hot water.
3. Load used for flexible heating.

The first two load types are fixed, while the last one is flexible, and the shape of the load profiles differ for different building categories.

We want to investigate the value of flexibility for different compositions of the building stock. To isolate the effect of flexibility activation on the total costs and other relevant indicators, we therefore need to keep the total energy required constant across cases with varying building compositions in the same period. Therefore, one of the building categories is chosen as the reference building and a scaling factor as described in eq. (35) is applied to generate an equivalent for the other categories. We use the TEK87 building as the reference, and compute the equivalent PH by multiplying the load profiles and thermal storage capability with the scaling factor to keep the energy use equal between cases.

$$\text{Scaling factor} = \frac{\text{total load of reference building}}{\text{total load of building category } \phi} \quad (35)$$

To investigate the impact of various scenarios, analyses are carried out for the months January and April for the year 2019. We find the scaling factor for the PH to be 2.93 in January and 2.16 in April. Since the PH standard is significantly more energy efficient than TEK87 buildings this order of magnitude is reasonable. It is also within expectations

---

[2] https://www.renewables.ninja/.

that the factor is lower in April than in January because the insulation level is the main driver for the load differences.

4. Results and discussion

4.1. Identification of building parameters

The parameter has been identified using the indoor temperature decay during 30 nights in January 2019. Results are reported in Table 3. As mentioned in section 2.4, U_{tot} is assumed known from methods based on in-situ measurements. As the test case is a virtual model in IDA ICE, we have identified U_{tot} using a step response of P_e leading to a $\Delta T_{i,\infty}$ of 2 °C [26]. This leads to a value of 50 W/K for the PH house and 120 W/K for the TEK87 house. In Alzetto et al. [42], the QUB method has an accuracy of about +/- 20%. Therefore, the influence of the uncertainty of U_{tot} on the other parameters is also reported in Table 3.

Palmer Real et al. [38] has identified the time constant of 39 houses in Denmark. τ_1 ranged between 20 and 90 h while τ_2 ranged between 5 and 45 minutes. It is in line with our results. The sensitivity analysis shows that τ_1 is the parameter that is the most affected to variations of U_{tot}. It is also worth noticing that the change of insulation level from TEK87 to PH has an influence on the value of all four parameters.

4.2. Load balancing through space heating flexibility

Now, the energy system model is run and the space heating flexibility is included according to the parameters identified in the previous

Table 3
Parameters identified for eq. (9) and eq. (10).

Case	U_{tot} [W/K]	τ_1 [h]	τ_2 [h]	α [-]
TEK87 (baseline)	120.0	32.7	0.252	0.83
TEK87 (+20%)	144.0	25.5	0.249	0.80
TEK87 (-20%)	108.0	43.6	0.254	0.86
PH (baseline)	50.0	90.6	0.431	0.90
PH (+20%)	60.0	73.1	0.430	0.88
PH (-20%)	40.0	116.8	0.432	0.92

section. In this section, we run the model with 5 TEK87 buildings and 5 PH building equivalents scaled according to the description in section 3.3 to keep the baseline energy use for the month equal for the building categories.

To assess the impact of optimizing the space heating flexibility potential, analyses are run both with optimization of the space heating flexibility and in a simulation mode without activating space heating flexibility. An overview of the main results for this initial assessment of load balancing through space heating flexibility is provided in Table 4. Note that for the KPI comparison, energy prices are divided into three categories to give an overview of arbitrage effects.[3]

There is a large difference in the total costs when we compare the winter and spring, which is mainly because of increased output from PV and lower load in the spring along with lower prices both for energy and capacity. Furthermore, looking at the impact of optimizing the heat load, the total system costs decrease when the heating flexibility is optimized, and the cost reduction is most prominent during the winter. In the winter, the grid capacity is relatively expensive, and the peak capacity usage is reduced 40.2% by utilizing the space heating flexibility. In comparison, there is a relatively low reduction of 17.9% of the peak load in April, which is because of the relatively low cost for capacity usage and the low potential for reducing the peak due to low heating needs.

Fig. 4 shows the operation of the space heating flexibility during the time period when the reference scenario has a total capacity usage of 58.4 kW observed during hour 223. Note that although there are relatively high short-term peaks under optimized heating, the total capacity usage is in reality lowered to 34.9 kW because it is averaged for each hour under the imposed billing structure. The occurrence of sub-hourly load peaks under the optimization of space heating is further elaborated in section 4.6.

Another contributor to the cost savings is shifting of the heat output towards hours with lower prices. This means that it is optimal to preheat the building during periods with lower prices or when there is available PV generation to reduce the heat output during high-price periods. The

---

[3] Low price is here defined as less than one third of the maximum price, medium price is higher than low price and less than two thirds of the maximum price, high price is higher than medium price.

Table 4
Comparison of KPIs when introducing space heating flexibility.

	January 2019		April 2019	
	Reference scenario	Optimized heating	Reference scenario	Optimized heating
System cost [EUR]	3 188.4	2 787.4	240.4	235.6
Grid capacity usage [kW]	58.4	34.9	27.9	24.9
Energy import [kWh]	21 319	22 121	5 066	4 906
Energy export [kWh]	0	0	4 310	3 978
Average import price [EUR/kWh]	0.0697	0.0679	0.0501	0.0501
Average export price [EUR/kWh]	N/A	N/A	0.0508	0.0510
Low price energy [kWh]	18 558	20 052	285	341
Medium price energy [kWh]	2 361	1 806	469	596
High price energy [kWh]	400	262	2	-10
Energy self-consumed [kWh]	586	586	4 507	4 770
Energy self-consumed [%]	100	100	51	55
TEK87 energy use [kWh]	10 952	11 140	4 786	4 889
PH energy use [kWh]	10 952	11 566	4 786	4 786
TEK87 thermal loading [kWh]	0	975	0	335
PH thermal loading [kWh]	0	3 380	0	0
TEK87 preheating losses [kWh]	0	188	0	103
PH preheating losses [kWh]	0	614	0	0
TEK87 avg. increase [°C]	0	0.42	0	0.24
PH avg. increase [°C]	0	1.13	0	0

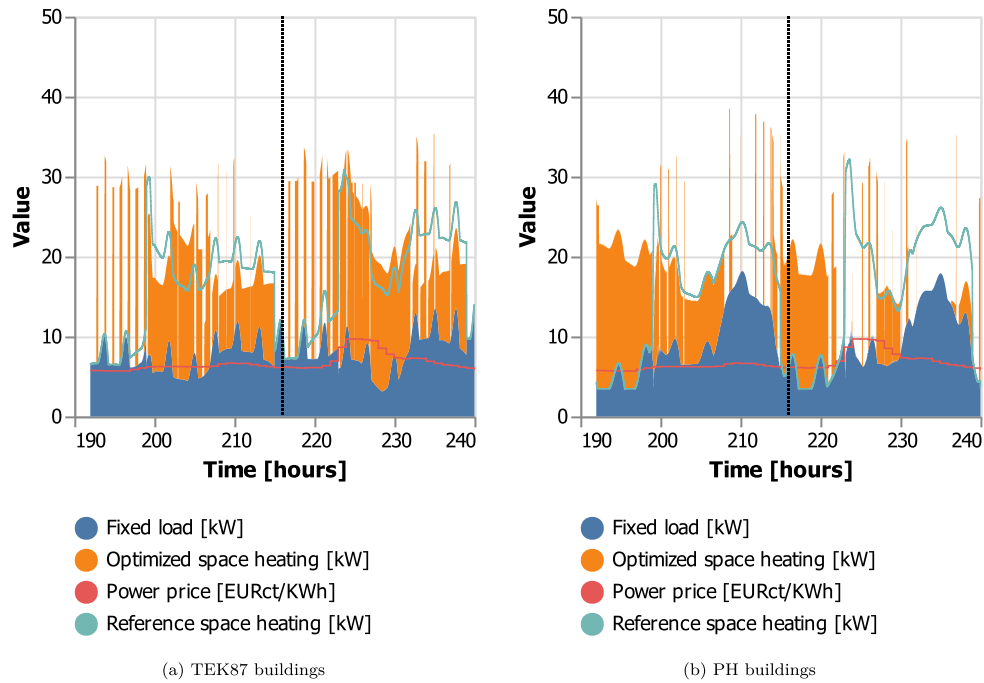(a) TEK87 buildings   (b) PH buildings

Fig. 4. Optimized and reference space heating load for the two building categories during January 8 (left of vertical dotted line) and 9 (right of vertical dotted line).

trade-off from this use of flexibility is the increase of total energy due to preheating losses. Preheating losses occur because increasing the indoor temperature above the reference temperature gives higher heat losses to the building's outdoor environment. The preheating losses for the winter are 188 kWh for the TEK87 category and 614 kWh for the PH category. These numbers might seem counter-intuitive since the TEK87 building standard is associated with higher energy losses due to inferior energy performance compared to the PH category. The explanation of the preheating loss "mystery" is that the TEK87 building is rarely preheated because it is more cost-effective to utilize the PH category as much as possible. Preheating PH give relatively low energy losses compared to a corresponding preheating under the TEK87 building standard. Hence, under the underlying assumption of no thermal discomfort within the allowed limits, the optimal outcome is to utilize PH for the bulk of the flexibility needs and only preheat the TEK87 buildings when the system really needs it.

4.3. Validation of optimized heating

The energy model enables computing the optimal change of the space-heating power (ΔP_e) compared to the reference scenario ($P_{e,ref}$). The resulting change of the indoor temperature (ΔT_i) is kept within comfortable indoor temperature limits by the energy model using the temperature prediction of the second-order thermal mass model identified in section 4.1. In order to investigate the prediction accuracy of this data-driven second-order model, the indoor temperature $\Delta T_i + T_{i,ref}$ computed by the second-order model can be compared to the indoor temperature that is obtained when the emitted power $\Delta P_e + P_{e,ref}$ is applied directly to the heat emitter in IDA ICE (i.e., an open-loop simulation with a direct control of the emitted power). The indicators to measure the prediction performance are the mean bias error (MBE), the normalized mean bias error (NMBE), the coefficient of variation of the room mean square error (CVRMSE) and the fitting based on the normalized room mean square error (NRMSE fitting). The higher the NRMSE fitting, the lower the simulation error. Results are reported for the TEK87 and PH houses in Table 5.

A sensitivity analysis is done by comparing the case where the second-order model was calibrated using an exact knowledge of U_{tot} with the case with an error of $+/- 20\%$ on U_{tot}. It enables investigating

Table 5
Prediction performance of the second-order model compared to the IDA ICE for January.

U_{tot}	PH			TEK87		
	Baseline	+20%	-20%	Baseline	+20%	-20%
MBE [°C]	0.19	0.029	0.35	0.24	0.012	0.55
NMBE [%]	0.86	0.12	1.57	1.15	0.059	2.67
CVRMSE [%]	1.25	1.9	2.0	2.6	3.3	3.4
NRMSE fitting [%]	69.0	35.7	63.9	66.0	57.5	68.6

how the prediction performance depends on an accurate identification of U_{tot} using field measurements. Time series of the indoor temperature predicted by the second-order model and IDA ICE for January are shown in Fig. 5. Even the linear second-order model is only based on the calibration of four parameters, it can be seen it is able to fairly reproduce the thermal dynamics of the indoor temperature of a detailed BPS tools (namely IDA ICE) over a period of two weeks. Using the exact U_{tot} for the parameter identification, the second-order model performs equally well for the PH and TEK87 houses. However, considering a potential error of 20% on U_{tot} does not impact significantly the prediction performance of the TEK87 house while an increase of 20% of U_{tot} decreases noticeably this performance for the PH. In conclusion, the proposed second-order model has a level of accuracy that is acceptable for energy planning models. However, with higher insulation level, the overall model performance depends more on the accuracy of the identified U_{tot}.

4.4. Effect of building category mix

The analysis of section 4.2 is extended by a sensitivity analysis on the building category mix, and the effect of increasing the energy share of PH from 0 to 100% is considered. The computations are done in 10% intervals by varying the amount of PH from 0 to 10 TEK87 building equivalents, and reducing the amount of TEK87 buildings accordingly to maintain a total building stock equivalent of 10 TEK87 buildings.
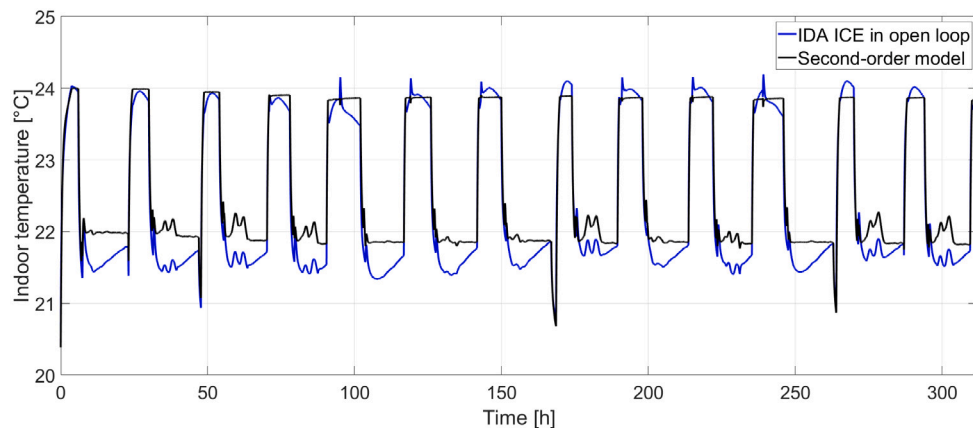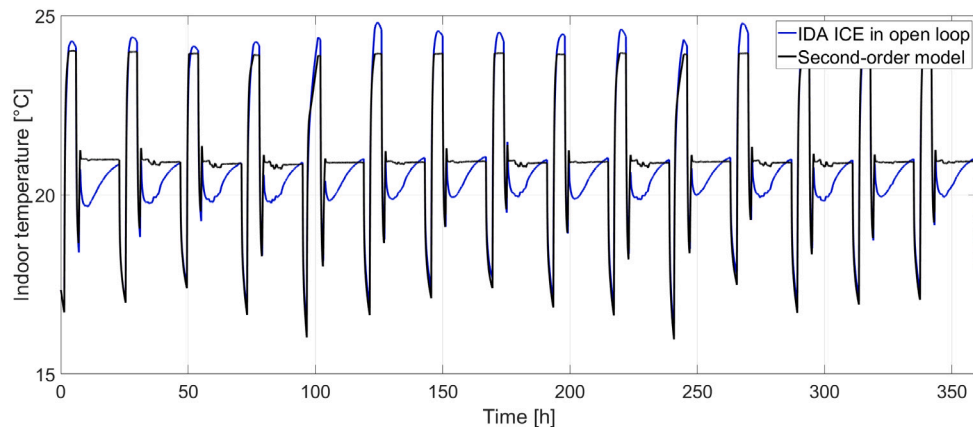
(a) PH buildings with baseline ($U_{tot} = 50W/K$).

(b) TEK87 buildings with baseline ($U_{tot} = 120W/K$).

Fig. 5. Indoor temperature of the second-order model compared to IDA ICE for the PH house in January using the exact U_{tot} for the parameter identification.

Fig. 6 plots the change of selected KPIs relative to the reference case. The reference case is a 50/50 mix, as assumed in section 4.2, where all plots intersect with a deviation of zero.

The KPI sensitivities reveal that the KPIs are improved in the sense of decreased total costs and peak load by an increase in the energy share of PH, but only to a certain extent. The threshold is at about 60-80%, where the costs and peak load increase again as the share of PH is increased beyond this point. Although PH is preferable from an energy flexibility point of view, the TEK87 buildings can bring value because they have some properties that complement the system.

4.5. Battery equivalent of space heating flexibility

The space heating flexibility is, within its limitations, able to adjust the load profile of the system under consideration. Another technology that can also be used for such flexibility provision is batteries. In the context of our case study, it is interesting to make a comparison between these options.

Table 6 provides an overview of four different cases for January. For the sake of comparison, the analysis is based on the case with a 50/50 mix of PH and TEK87 as used in section 4.2, and the first two cases are equivalent to the initial results with and without the use of space heating flexibility. Next, the battery equivalent of the space heating flexibility is computed. To compute the battery equivalent of the space heating flexibility, the optimization problem is modified to minimize the battery size needed to obtain the same total costs. To investigate potential interactions, the last case includes both the identified battery equivalent and the space heating flexibility.

For the purpose of cost decreases in line with the building flexibility potential, the battery equivalent is 79.1 kWh for the system under consideration. In comparison, a Tesla Powerwall is 13.5 kWh.[4] It can also be observed that the optimization of space heating flexibility decreases the peak load more than the battery equivalent. Observing the energy purchased in the different price segments, it seems to be optimal for the battery to rely more on price arbitrage to achieve the required cost reduction.

When both the battery equivalent and the space heating flexibility are operated together, the KPIs improve beyond what is possible with each individually. Both costs and the required grid capacity decreases, while shifting energy use towards the low price periods. An interesting observation is that the battery is used more when the space heating flexibility is also included while the use of space heating flexibility is reduced. Hence, the combination of these flexibility assets is beneficial and the presence of space heating flexibility is an enabler for the battery profitability rather than a competitor.

Fig. 7 provides plots to compare the operational patterns of the four cases for the period that gives the initial peak load of the system in January. First, Fig. 7a plots how the grid capacity usage fluctuates when no flexibility can be operated. By operating the space heating flexibility in Fig. 7b the grid capacity usage is more stable, and the peak usage is significantly decreased. The plot includes the thermal deviation of the buildings to show how the buildings are loaded and unloaded to reduce the system's total load when needed.

---

4 https://www.tesla.com/powerwall.

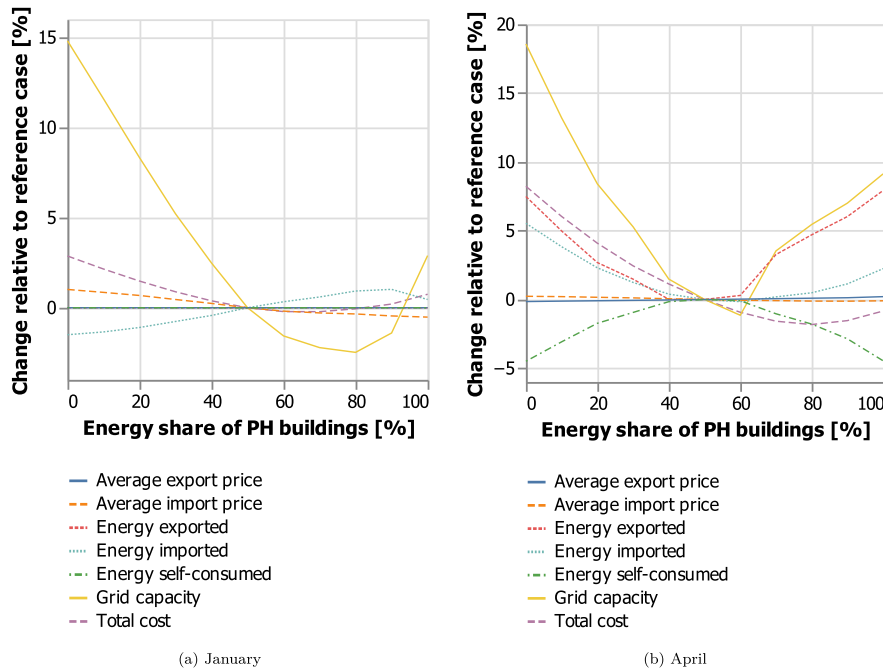(a) January   (b) April

Fig. 6. Sensitivity of key KPIs to building category mix for January and April in 2019. Results are shown relative to the case with 50% TEK87 and 50% PH (reference case). Curves are linearly fitted based on results when the share of PH is increased in 10% intervals.

Table 6
Comparison of selected KPIs with battery equivalent in January.

	Reference scenario	Optimized heating	Battery equivalent	Both
System cost [EUR]	3 188.4	2 787.4	2 787.4	2 696.4
Grid capacity usage [kW]	58.4	34.9	37.9	31.9
Battery capacity [kWh]	0	0	79.1	79.1
Energy import [kWh]	21 319	22 121	21 559	21 878
Average import price [EUR/kWh]	0.0697	0.0679	0.0678	0.0673
Low price energy [kWh]	18 558	20 052	19 568	20 070
Medium price energy [kWh]	2 361	1 806	1 752	1 595
High price energy [kWh]	400	262	239	213
TEK87 energy use [kWh]	10 952	11 140	10 952	10 978
PH energy use [kWh]	10 952	11 566	10 952	11 211
TEK87 thermal loading [kWh]	0	975	0	209
PH thermal loading [kWh]	0	3 380	0	1 621
Battery charging [kWh]	0	0	2 353	2 547
TEK87 preheating losses [kWh]	0	188	0	25
PH preheating losses [kWh]	0	614	0	259
Battery energy losses [kWh]	0	0	240	275
TEK87 avg. increase [°C]	0	0.42	0	0.06
PH avg. increase [°C]	0	1.13	0	0.47

The battery equivalent is the sole provider of flexibility in Fig. 7c and plots the battery storage level along with the grid capacity usage. Compared to the initial situation without any flexibility assets, the grid capacity usage is flattened, but it fluctuates more than in the situation of only space heating flexibility.

Co-optimization of space heating flexibility and the battery equivalent is the basis for Fig. 7d. When both flexibility assets are included, the grid capacity usage becomes almost constant. When space heating flexibility can provide flexibility, the battery is kept at a higher storage level in preparation of the unloading event right before time step 240. Also, in line with the KPI results, the space heating flexibility is used more sparingly. The reduction in the use of space heating flexibil-

ity is most prominent for the TEK87 buildings since this category has less insulation and relatively higher preheating losses.

4.6. Price arbitrage effects

As was observed from Fig. 4, there are frequent short-term load spikes. These occur as the result of the flexibility optimization being run with a higher resolution than the resolution of the price signal. First, the flexibility is optimized with a timestep of 0.02 hours, while the energy price is updated with an hourly timestep. When the energy price increases from one timestep to another, it will be beneficial to "shock-preheat" the building right before the price is increased. This pattern can be observed in Fig. 8 where the TEK87 house takes advan-
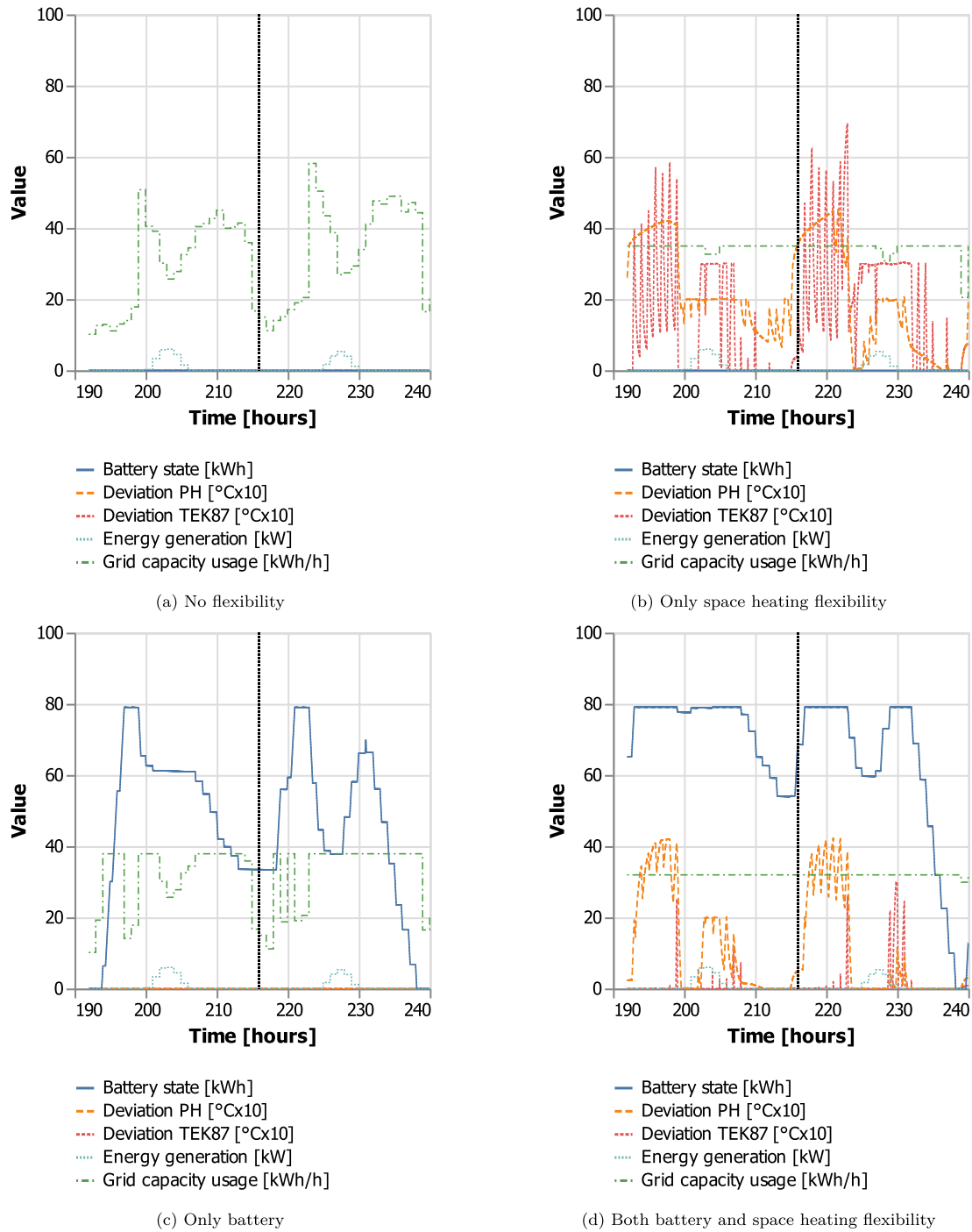
(a) No flexibility

(b) Only space heating flexibility

(c) Only battery

(d) Both battery and space heating flexibility

Fig. 7. Flexibility operation for January 8 (left of vertical dotted line) and 9 (right of vertical dotted line) showing operation of flexible assets together with the measured grid capacity usage.

tage of the lower price during time step 558 to preheat the building during almost the entire hour. On the other hand, the PH category concentrates the preheating to occur right before the price increase in time step 559. The same effect can be observed for both buildings at the end of time step 559 when the price increases even further during time step 560. This pattern takes advantage of energy arbitrage possibilities while limiting the preheating losses.

From a system planner's perspective such as the distribution grid company, energy flexibility optimization with higher temporal resolution than the price signal might give undesirable effects because of short-term load spikes. Such "shock-preheating" would not be a prob-

lem if the preheating for different buildings is randomly distributed in time, but in this case the incentives in place would coordinate the load spikes. For instance, if many buildings in an area are "shock-preheating" right before the energy price increases, the load spikes of the different buildings would coincide because they are exposed to the same price signal. Such issues are not necessarily resolved through a capacity-based tariff either since the billable capacity is measured as the hourly average. Hence, the capacity usage can be very high for a few minutes without significantly increasing the billable capacity. A higher resolution of the price signal (e.g., 15 minutes) could reduce this issue, but the underlying problem remains the same when the flexibility activa-
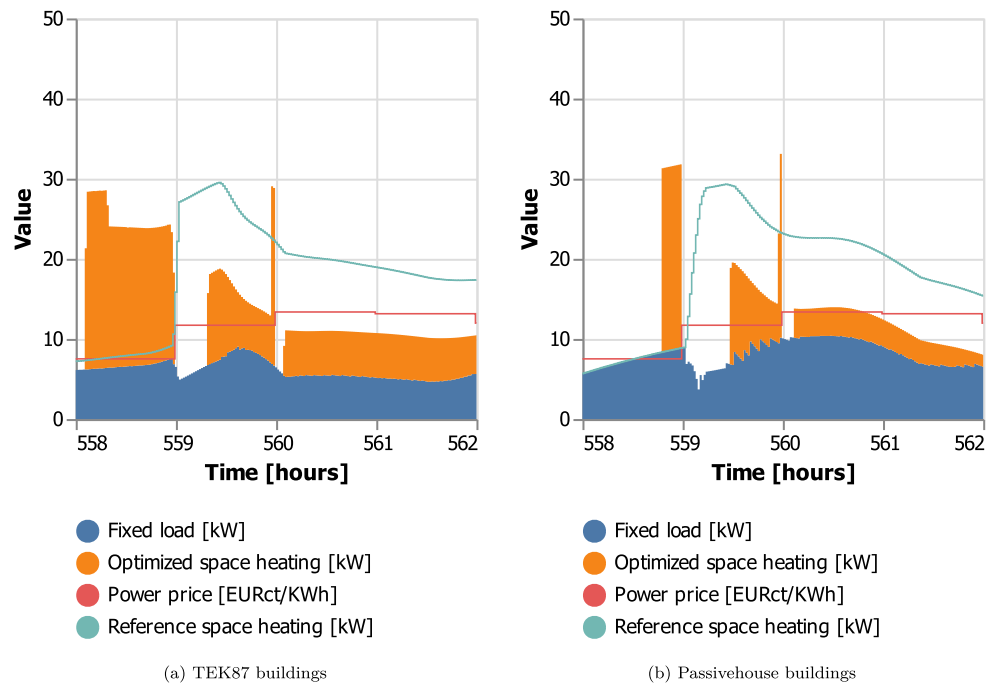
(a) TEK87 buildings

(b) Passivehouse buildings

Fig. 8. Optimized and reference space heating load for the two building categories for hours with prominent energy arbitrage effects.

tion is optimized with a higher resolution than the resolution of the price signal.

5. Conclusion

5.1. Conclusion

To include the potential of space heating flexibility in energy system models, this article provides a space heating flexibility formulation to represent the flexibility potential of the heat load profile in relative terms. A linear data-driven formulation for thermal mass activation is provided, validated against a nonlinear simulation model, and its application is demonstrated by including it as part of an energy system optimization problem. The linearized thermal mass model is included in an illustrative case study to optimize the flexibility operation as a part of a local energy system with buildings of two efficiency levels and local energy generation. Also, the method gives a framework to compare the thermal mass energy storage of buildings with batteries.

Based on the findings of this paper, it can be concluded that the method enables to analyze the aggregated energy flexibility of several residential buildings with different insulation levels at a limited computational cost. The provided model fits well in the context of energy system planning and optimization since it is able to represent the potential for deviating from a predefined load profile with a limited need for input data to characterize the flexibility.

The conducted case study provides insight regarding the operation of space heating flexibility and the influence of highly-insulated and poorly insulated houses in the energy flexibility portfolio. The results confirm that thermal mass flexibility has potential to provide peak load reductions and energy arbitrage effects to lower the total costs for operating energy systems with the potential drawback of increased energy use due to building preheating with the associated thermal losses. Buildings with a higher insulation level are loaded more frequently due to their lower storage losses compared to less insulated building. However, some presence of less insulated buildings seems to be preferable since they diversify the operational portfolio. The energy storage capacity of the building thermal mass is evaluated against batteries, and the potential of thermal mass flexibility is significant when compared to its equivalent battery storage.

5.2. Limitations and further work

First, the building flexibility is compared against batteries in this article to compare the flexibility potential, but without considering technology investment costs. It is worth noting that batteries are a relatively expensive technology for large-scale energy storage (see e.g. [58]). Also, other heat storage options may be cost-effective compared to passive heat storage in buildings [59]. Therefore, it can be interesting for further work to consider a wider range of technologies and also their investment costs. By applying several technologies in the same modeling framework, it would be possible to identify their relative cost-effectiveness, and also potential synergies. Hence, the effect of thermal mass activation on the optimal system configuration is a topic that can be studied more comprehensively and in greater detail.

Second, the provided energy system case study relies on a limited amount of building categories to demonstrate the developed model. Thermal mass activation can be applied more comprehensively in energy system analyses by including more building types according to the building stock of an area.

Third, the proposed model could be adapted for real-time operation purposes or short-term planning. It is therefore relevant for further work to consider other types of application by adapting the model or combining it with other approaches. The prediction performance of the proposed second-order model should be further investigated on other building types, also with test cases where the building should be modeled as multi-zone.

Finally, we specify thermal deviation limits and do not include a cost for thermal discomfort in our model. Since our model optimization uses PH to shift energy for longer time periods, thermal discomfort costs would reduce the optimal duration of temperature deviations. In this regard, the effect of thermal discomfort on the optimization outcome can be investigated further.

Declaration of competing interest

The authors declare that they have no known competing financial interests or personal relationships that could have appeared to influence the work reported in this paper.

Data availability

Data will be made available on request.

Acknowledgement

This paper has been written within the Research Centre on Zero Emission Neighbourhoods in Smart Cities (FME ZEN). The authors gratefully acknowledge the support from the ZEN partners and the Research Council of Norway.

References

[1] Andrey Christopher, Fournié Laurent, Gabay Michaël, de Sevin Hugo. The role and need of flexibility in 2030: focus on energy storage. Technical report. European Commission; 2016.

[2] Jensen Søren Østergaard, Marszal-Pomianowska Anna, Lollini Roberto, Pasut Wilmer, Knotzer Armin, Engelmann Peter, et al. IEA EBC annex 67 energy flexible buildings. Energy and Buildings 2017;155(2017):25–34.

[3] Geidl Martin, Andersson Goran. Operational and structural optimization of multi-carrier energy systems. Eur. Trans. Electr. Power 2006;16(5):463–77.

[4] Orehounig Kristina, Mavromatidis Georgios, Evins Ralph, Dorer Viktor, Carmeliet Jan. Towards an energy sustainable community: an energy system analysis for a village in Switzerland. Energy and Buildings 2014;84:277–86.

[5] Orehounig Kristina, Evins Ralph, Dorer Viktor. Integration of decentralized energy systems in neighbourhoods using the energy hub approach. Appl. Energy 2015;154:277–89.

[6] Pinel Dimitri, Bjarghov Sigurd, Korpås Magnus. Impact of grid tariffs design on the zero emission neighborhoods energy system investments. In: 2019 IEEE Milan PowerTech; 2019. p. 1–6.

[7] Haupt Leon, Schöpf Michael, Wederhake Lars, Weibelzahl Martin. The influence of electric vehicle charging strategies on the sizing of electrical energy storage systems in charging hub microgrids. Appl. Energy 2020;273.

[8] Sadeghi Hadi, Rashidinejad Masoud, Moeini-Aghtaie Moein, Abdollahi Amir. The energy hub: an extensive survey on the state-of-the-art. Appl. Therm. Eng. 2019;161.

[9] Maroufmashat Azadeh, Taqvi Syed Taha, Miragha Amir, Fowler Michael, Elkamel Ali. Modeling and optimization of energy hubs: a comprehensive review. Inventions 2019;4(50).

[10] Dominković Dominik Franjo, Junker Rune Grønborg , Lindberg Karen Byskov, Madsen Henrik. Implementing flexibility into energy planning models: soft-linking of a high-level energy planning model and a short-term operational model. Appl. Energy 2020;260:114292.

[11] Vandermeulen Annelies, Reynders Glenn, Van Der Heijde Bram, Vanhoudt Robbe Salenbien, Saelens Dirk, Helsen Lieve. Sources of energy flexibility in district heating networks: building thermal inertia versus thermal energy storage in the network pipes. In: Proceedings of the urban energy simulation conference 2018. University of Strathclyde; 2018.

[12] Kensby Johan, Trüschel Anders, Dalenbäck Jan Olof. Potential of residential buildings as thermal energy storage in district heating systems - results from a pilot test. Appl. Energy 2015;137:773–81.

[13] Reynders Glenn, Diriken Jan, Saelens Dirk. Generic characterization method for energy flexibility: applied to structural thermal storage in residential buildings. Appl. Energy 2017;198:192–202.

[14] Du Baoxiang, Verbic Gregor, Fletcher John. Thermal modelling for demand response of residential buildings. In: 2017 Australasian Universities Power Engineering Conference, AUPEC 2017, 2017, Novem 1–6, 2018.

[15] Weiß Tobias, Fulterer Anna Maria, Knotzer Armin. Energy flexibility of domestic thermal loads–a building typology approach of the residential building stock in Austria. Adv. Build. Energy Res. 2019;13(1):122–37.

[16] Chen Yongbao, Xu Peng, Chen Zhe, Wang Hongxin, Sha Huajing, Ji Ying, et al. Experimental investigation of demand response potential of buildings: combined passive thermal mass and active storage. Appl. Energy 2020;280:115956.

[17] Fernández Carlos Bandera, Pachano Jose, Salom Jaume, Peppas Antonis, Ruiz Germán Ramos. Photovoltaic plant optimization to leverage electric self consumption by harnessing building thermal mass. Sustainability (Switzerland) 2020;12(2).

[18] Marotta Ilaria, Guarino Francesco, Cellura Maurizio, Longo Sonia. Investigation of design strategies and quantification of energy flexibility in buildings: a case-study in southern Italy. J. Build. Eng. 2021;41:102392.

[19] Mathiesen BV, Lund H, Connolly D, Wenzel H, Ostergaard PA, Möller B, et al. Smart energy systems for coherent 100% renewable energy and transport solutions. Appl. Energy 2015;145:139–54.

[20] Le Dréau J, Heiselberg P. Energy flexibility of residential buildings using short term heat storage in the thermal mass. Energy 2016;111:991–1002.

[21] Romanchenko Dmytro, Kensby Johan, Odenberger Mikael, Johnsson Filip. Thermal energy storage in district heating: centralised storage vs. storage in thermal inertia of buildings. Energy Convers. Manag. January 2018;162:26–38.

[22] Dominković DF, Gianniou P, Münster M, Heller A, Rode C. Utilizing thermal building mass for storage in district heating systems: combined building level simulations and system level optimization. Energy 2018;153:949–66.

[23] Junker Rune Grønborg, Azar Armin Ghasem, Lopes Rui Amaral, Lindberg Karen Byskov, Reynders Glenn, Relan Rishi, et al. Characterizing the energy flexibility of buildings and districts. Appl. Energy 2018;225:175–82.

[24] Junker Rune Grønborg, Kallesøe Carsten Skovmose, Real Jaume Palmer, Howard Bianca, Lopes Rui Amaral, Madsen Henrik. Stochastic nonlinear modelling and application of price-based energy flexibility. Appl. Energy 2020;275:115096.

[25] Joe Jaewan, Dong Jin, Munk Jeffrey, Kuruganti Teja, Cui Borui. Virtual storage capability of residential buildings for sustainable smart city via model-based predictive control. Sustain. Cities Soc. 2021;64:102491.

[26] Georges Laurent, Storlien Elin, Askeland Magnus, Lindberg Karen Byskov. Development of a data-driven model to characterize the heat storage of the building thermal mass in energy planning tools. In: E3S web of conferences, vol. 246; 2021.

[27] Brahman Faeze, Honarmand Masoud, Jadid Shahram. Optimal electrical and thermal energy management of a residential energy hub, integrating demand response and energy storage system. Energy Build. 2015;90:65–75.

[28] Guelpa Elisa, Deputato Stefania, Verda Vittorio. Thermal request optimization in district heating networks using a clustering approach. Appl. Energy 2018;228:608–17.

[29] Saletti Costanza, Gambarotta Agostino, Morini Mirko. Development, analysis and application of a predictive controller to a small-scale district heating system. Appl. Therm. Eng. 2020;165:114558.

[30] Ghilardi Lavinia Marina Paola, Castelli Alessandro Francesco, Moretti Luca, Morini Mirko, Martelli Emanuele. Co-optimization of multi-energy system operation, district heating/cooling network and thermal comfort management for buildings. Appl. Energy 2021;302.

[31] Salpakari Jyri, Rasku Topi, Lindgren Juuso, Lund Peter D. Flexibility of electric vehicles and space heating in net zero energy houses: an optimal control model with thermal dynamics and battery degradation. Appl. Energy 2017;190:800–12.

[32] Nguyen Duong Tung, Le Long Bao. Joint optimization of electric vehicle and home energy scheduling considering user comfort preference. IEEE Trans. Smart Grid 2014;5(1):188–99.

[33] Baader Florian Joseph, Mork Maximilian, Xhonneux André, Müller Dirk, Bardow André, Dahmen Manuel. Mixed-integer dynamic scheduling optimization for demand side management. Proceedings of the 30 European symposium on computer aided process engineering, vol. 48. Elsevier Masson SAS; 2020. p. 1405–10.

[34] Patteeuw Dieter, Bruninx Kenneth, Arteconi Alessia, Delarue Erik, D'haeseleer William, Helsen Lieve. Integrated modeling of active demand response with electric heating systems coupled to thermal energy storage systems. Appl. Energy 2015;151:306–19.

[35] Patteeuw Dieter, Helsen Lieve. Combined design and control optimization of residential heating systems in a smart-grid context. Energy Build. 2016;133:640–57.

[36] Hedegaard Rasmus Elbaek, Friedrichsen Lewe, Tougaard Janus, Mølbak Tommy, Petersen Steffen. Building energy flexibility as an asset in system-wide district heating optimization models. In: uSIM2020; 2020.

[37] Madsen H, Holst J. Estimation of continuous-time models for the heat dynamics of a building. Energy Build. 1995;22:67–79.

[38] Palmer Real Jaume, Rasmussen Christoffer, Li Rongling, Leerbeck Kenneth, Jensen Ole Michael, Wittchen Kim B, et al. Characterisation of thermal energy dynamics of residential buildings with scarce data. Energy and Buildings 2021;230.

[39] Bacher Peder, Madsen Henrik. Identifying suitable models for the heat dynamics of buildings. Energy and Buildings 2011;43(7):1511–22.

[40] Madsen Henrik, Bacher Peder, Bauwens Geert, Deconinck An-Heleen, Reynders Glenn, Roels Staf, Himpe Eline, Lethé Guillaume. Thermal performance characterization using time series data – statistical guidelines. Technical report. Belgium: KU Leuven; 2016.

[41] Bauwens Geert, Roels Staf. Co-heating test: a state-of-the-art. Energy Build. 2014;82:163–72.

[42] Alzetto Florent, Pandraud Guillaume, Fitton Richard, Heusler Ingo, Sinnesbichler Herbert. QUB: a fast dynamic method for in-situ measurement of the whole building heat loss. Energy Build. 2018;174:124–33.

[43] Bjorvatn Bjørn, Mrdalj Jelena, Saxvig Ingvild W, Aasnæs Tom, Pallesen Ståle, Waage Siri. Age and sex differences in bedroom habits and bedroom preferences. Sleep Med. 2017;32:157–61.

[44] Hensen Jan LM, Roberto Lamberts, editors. Building performance simulation for design and operation. 2nd edition. Routhledge; 2019.

[45] Bezanson Jeff, Edelman Alan, Karpinski Stefan, Shah Viral B. Julia: a fresh approach to numerical computing. SIAM Rev. 2017;59(1):65–98.

[46] Carlson Fredrik Bagge, Fält Mattias. Controlsystems.jl: a control systems toolbox for Julia; 2016.

[47] EQUA. IDA indoor climate and energy 4.8; 2020.

[48] Rønneseth Øystein, Sartori Igor. Method for modelling Norwegian single-family houses in IDA ICE. ZEN Memo 10. 2018.

[49] Storlien Elin. Characterizing the demand response potential of thermal heat load in buildings; 2020.

[50] Standard Norge. NS 3700:2010 criteria for passive houses and low energy buildings – residential buildings; 2010.

[51] Byggeforskrift Kommunaldepartementet. 1987, 1987.

[52] Chen Qingyan. Ventilation performance prediction for buildings: a method overview and recent applications. Build. Environ. 2009;44(4):848–58.

[53] Standard Norge. SN/TS 3031:2016 energy performance of buildings - calculation of energy needs and energy supply; 2016.

[54] Elvia Historical Market Data. https://www.elvia.no/nettleie/alt-om-nettleie/historiske-priser-pa-nettleie-i-oslo-og-viken/. [Accessed January 2022].

[55] NordPool Historical Market Data. https://www.nordpoolgroup.com/historical-market-data/. [Accessed January 2022].

[56] Tax rate for electricity 2019. https://www.skatteetaten.no/en/rates/electricity/?year=2019#rateShowYear. [Accessed January 2022].

[57] Pfenninger Stefan, Staffell Iain. Long-term patterns of European PV output using 30 years of validated hourly reanalysis and satellite data. Energy 2016;114:1251–65.

[58] Lund Henrik, Østergaard Poul Alberg, Connolly David, Ridjan Iva, Mathiesen Brian Vad, Hvelplund Frede, Thellufsen Jakob Zinck, et al. Energy storage and smart energy systems. Int. J. Sustain. Energy Plan. Manag. 2016;11:3–14.

[59] Hedegaard Karsten, Mathiesen Brian Vad, Lund Henrik, Heiselberg Per. Wind power integration using individual heat pumps - analysis of different heat storage options. Energy 2012;47(1):284–93.